The Journal of Neuroscience

Spectral modulation and co-modulation of independent EEG activities

Journal:	*Journal of Neuroscience*
Manuscript ID:	draft
Manuscript Type:	Regular Manuscript
Manuscript Section:	Behavioral System Cognitive
Date Submitted by the Author:	n/a
Complete List of Authors:	Onton, Julie; UCSD, INC-Swartz Center Makeig, Scott; UCSD, INC-Swartz Center
Keywords:	Independent component analysis (ICA), Alpha, Beta, Brainstem, Cognition, Connectivity, Eeg [Electro-Encephalogram], Gamma, Human, Neuromodulation, single trial analysis, Synchronization
Themes & Topics:	b. Oscillations and synchrony < 9. Network Interactions < Theme B: Neural Excitability, Synapses, and Glia: Cellular Mechanisms, a. Perception and imagery < 1. Human Cognition, Behavior, and Anatomy < Theme E: Cognition and Behavior

Spectral modulation and co-modulation of independent EEG activities

Julie Onton* & Scott Makeig

Institute for Neural Computation
University of California San Diego
9500 Gilman Drive
La Jolla CA 92093-0961

January 30, 2007

Email: {julie,scott}@sccn.ucsd.edu

* Corresponding author

The ms. contains 7 figures (Figs. 1-7) and no tables

Abstract: 248 words
Introduction: 498 words
Methods: 2650 words
Results: 1746 words
Discussion: 1500 words
References: 62

Supplement: pdf text including 5 figures (Figs. S1-S5)

Abstract

Power spectra of human electroencephalographic (EEG) data exhibit large moment-to-moment fluctuations across a broad frequency range. Here, we report first results of log-linear decomposition of these fluctuations into independent modulator (IM) processes acting on one or more parts of the power spectra of one or more maximally independent component (IC) processes separated from the data by independent component analysis (ICA). From data of 34 subjects performing an emotion imagination task, we decomposed second-to-second changes in log spectrograms of ICs with dipolar scalp maps by infomax ICA, producing 15 IMs per subject each accounting for distinct spectral fluctuations in one or more IC processes. Three types of IMs were well represented across subjects, each scaling IC power either in predominantly bilateral spindle activity at an (8-12 Hz) alpha-band frequency and its harmonics, in some portion of the (13-35 Hz) beta band, or smoothly across a broad frequency range, most strongly at high frequencies (often extending to at least 125 Hz). Such broadband IMs either, (a) modulated the balance of low- versus high-frequency activity across the cortex, with a mean fulcrum near 25 Hz, resembling EEG changes associated with arousal, (b) spatially redistributed power above 10 Hz among several ICs, or else (c) modulated power above 5 Hz of a single IC. In analyses including ICs accounting for scalp muscle activity, cortical broadband ICs were distinct from electromyographic (EMG) modulations. We speculate that the characteristic modes of spectral modulation identified here may index separable actions of known cortical neuromodulatory systems.

Introduction

A dominant feature of the human EEG is its strong second-to-second variability, periods of clear oscillatory activity alternating irregularly with other, less clearly ordered activity. Oscillations produce peaks in the mean EEG power spectrum, which otherwise decreases smoothly as frequency increases. EEG spectral dynamics are complex: peak alpha frequencies of the summed sources may differ across subjects, times, and scalp locations (Andrew and Pfurtscheller, 1997). Bi-harmonic alpha and beta band (13-30 Hz) spectral peaks often occur together, most clearly in the 'mu-rhythm' spindles that appear over sensorimotor cortex between infrequent intended movements (Leocani et al., 1997), while solo beta-band activity increases directly following movement offset (Jurkiewicz et al., 2006). High-frequency gamma band (30-80 Hz) activity is typically not periodic but broadband (Freeman, 2004), and still higher gamma (80-200 Hz) is observed in electrocorticographic (ECOG) field activity during information processing in relevant cortical areas (Crone et al., 1998).

Mean EEG spectral changes often accompany changes in state, task, and performance. For example, changes in alpha band power may index changes in attention (Worden et al., 2000) and changes in alpha frequency may relate to task differences (Klimesch et al., 1997; Klimesch et al., 1998). Beta-band activities are associated with focused attention (Wrobel, 2000), and mean gamma band power is stronger during alert performance (Makeig and Jung, 1996), suggesting an association with attention, and conscious awareness (Fries et al., 2001; Cantero et al., 2004), as well as 'binding' of stimulus attributes (Singer and Gray, 1995; Herculano-Houzel et al., 1999). However, trial-to-trial spectral fluctuations may dominate such mean changes (Onton et al., 2005).

Scalp EEG analysis is further complicated by the fact that oscillatory activity recorded at a single scalp channel, for example in the (8-12 Hz) alpha band, typically sums activities from several cortical source areas separated as widely as occipital and sensorimotor cortex (Makeig et al., 2002). To accurately model the relation of EEG dynamics to behavior and experience, activities of single cortical EEG source areas must first be isolated. Independent component analysis (ICA) decomposes scalp-recorded EEG data into the weighted sum of maximally temporally independent component (IC)

processes (Makeig, 1996). Under favorable circumstances, the scalp projections of many ICs are compatible with generation by partially-synchronous local field activity within a single cortical patch. However, spectral shifts often concurrently affect multiple ICs, suggesting they might reflect actions of more widely distributed control processes, including the brainstem-based neuromodulatory systems using dopamine, acetylcholine, norepinephrine, etc. (Robbins, 1997; Bardo, 1998).

Studies of EEG spectral dynamics typically consider separate narrow frequency bins or pre-defined frequency bands. To better understand the roles of field dynamics in brain function, models of spectral dynamics derived from the data themselves are desirable. Recently, we showed that spectral activity of ICs projecting to the frontal midline exhibit discrete modes of event-related power modulation during a working memory task (Onton et al., 2005). Here, we demonstrate a related method for decomposing spectral fluctuations of multiple ICs into the product of distinct spectral modulator and co-modulator processes.

Methods

Subjects and Task. Thirty four young adult volunteers participated in the experiment (14 male, 20 female; age range, 18-38 years, age mean and standard deviation, 25.5 ± 5 years). Subjects were seated comfortably with eyes closed in a dimly lit room with air-tube fed ear-bud earphones. Imagination of emotional states was encouraged and guided by a set of pre-recorded verbal narratives. Each session began and ended with two minutes of eyes closed silent rest. The task then began with a recorded explanation of the task, followed by approximately five minutes of guided imagery relaxation instructions to promote a relaxed, inwardly-focused state. Guided imagery narratives for fifteen successive emotions, separated by relaxation interludes, were then presented. To minimize subject stress, the emotion sequence was chosen to alternate pseudo-randomly positive emotions (love, joy, happiness, relief, compassion, contentedness, excitement, awe) with negative emotions (anger, jealousy, disgust, frustration, fear, sadness, grief).

Each (15-30 s) pre-recorded emotional imagery induction began with a short description of the emotion and suggestions of one or more circumstances in which the target emotion might be vividly experienced, accompanied by suggestions to pay

attention to somatic sensations commonly associated with the emotion. The subject was encouraged to employ whatever imagery seemed suitable for stimulating a vivid and embodied experience of the suggested emotion.

Subjects were asked to take as much time as they needed to recall or imagine a scenario that would induce an experience of the suggested emotion. Eight of the subjects indicated the onset of the suggested emotion by pressing a right-hand button. Twelve other subjects made pulsating button presses on a pressure sensitive key, attempting to communicate the quality of the feeling they were experiencing. Fourteen other subjects were asked to press the button sporadically only at moments when they experienced a surge in the target emotion. Results for the three button-press subgroups of the analysis reported here proved similar, so for the purposes of this report the data of all 34 subjects were considered together.

Subjects were asked to attempt to experience each suggested emotion for three to five minutes. All subjects pressed a second, left-hand button when the experience of the emotion subsided, initiating a new relaxation instruction followed, after a 15 sec relaxation period, by the next emotion induction.

After the session, subjects completed a written debriefing questionnaire, first commenting on their overall experience in the experiment, then on their specific experiences during each of the suggested emotions, also estimating numerically the intensity and vividness of each emotion. Most of the 34 subjects whose data were analyzed here indicated they had enjoyed participating in the experiment, some expressing surprise at the relative ease with which they could vividly experience a fairly wide range of emotions in a single session, guided only by brief verbal suggestions.

Many of the subjects reported that one or two of the 15 emotions were more difficult for them to experience than others. The natures of these emotions varied across subjects. Only one subject indicated that, despite his efforts to self-induce an experience of each emotion, he experienced none of them vividly. All subjects were nevertheless included in the present analysis since our intention here was to study EEG spectral changes during eyes-closed imagery, which all subjects reporting performing successfully.

Data acquisition. EEG data were collected synchronously from 250 scalp, four infra-ocular, and two electrocardiographic (ECG) electrodes with an active reference (Biosemi ActiveTwo, Amsterdam) at a sampling rate of 256 Hz and 24-bit A/D resolution. Onsets and offsets of each guided imagery narrative, as well subject button presses were recorded in a simultaneously acquired event channel. Caps with a custom whole-head montage were used to position the electrodes, which were pressed into plastic wells in an electrode cap filled with water-based conductive gel. The recording montage covered most of the skull, forehead, and lateral face surface, omitting chin and fleshy cheek areas. The whole-head coverage and multiple chin straps, as well as the active recording technique that eliminated the need to scrape the skin surface, made the process of fitting and wearing the electrodes generally comfortable for the subjects. Locations of the electrodes relative to skull landmarks were recorded (Polhemus, Inc.).

Data analysis. Here, we present first results of a new method for decomposing fluctuations in EEG independent component (IC) power spectra into independent modes of co-modulation. The method was applied to normalized IC activity spectra during the 15 active emotion imagery periods from each subject.

Data preprocessing. Separating independent modes of spectral modulation involved several steps, detailed below. Data were analyzed by custom Matlab (The Mathworks, Inc.) analysis scripts built on the open source EEGLAB toolbox (Delorme, 2004). After re-referencing to digitally linked mastoids, the data were digitally filtered to emphasize frequencies above 1 Hz and below 50 Hz. Data periods containing broadly distributed, high-amplitude muscle noise and other irregular artifacts were identified by tests for high kurtosis or low probability activity and removed from analysis (Delorme, In press). Occurrence of eye blink, other eye movement, or isolated muscle noise artifact was not a criterion for rejection. Electrodes with poor skin contact, judged by their abnormal activity patterns, were also removed from the data, leaving 180-254 channels per subject (243 ± 16, mean ± std. dev.)

ICA decomposition. Remaining data time windows were then concatenated and submitted to decomposition by extended infomax ICA using the *binica* function (Makeig et al., 1997) available with the EEGLAB toolbox (http://sccn.ucsd.edu/eeglab). Infomax ICA finds a matrix, **W**, that linearly unmixes the original EEG channel data, **x**, into a sum of maximally temporally independent, and spatially fixed components, **u**, such that **u** = **Wx**. The rows of the resulting 'activation' matrix, **u,** are the independent component activities or activations, and its columns, the time points of the input data. Columns of the inverse matrix, $\mathbf{W}^{-1}$, give the relative projection weights from each independent component to each scalp electrode. For the derivation of the infomax algorithm, see (Jung, 2001); for practical details of its application to EEG data see (Makeig et al., 2004; Onton and Makeig, 2006).

Decompositions used default extended-mode *binica* training parameters with a stopping weight change of 1e-7. Extended infomax ICA (Lee et al., 1999) was used to allow recovery of any components with sub-gaussian activity distributions, including 60-Hz line noise contamination. The amount of data decomposed for each subject amounted to between 25 and 57 min (mean ± std. dev. points: 667k ± 115k). The scalp data were first reduced to between 90 and 160 principal dimensions, depending on data length and quality, using principal component analysis (PCA). The scalp data decomposed by ICA then comprised, on average, 64 time points (range, 26-87) for each weight in the square ICA unmixing matrix learned from the PCA-reduced data.

Independent component selection. IC activations from each subject were first assessed and categorized as brain activity or non-brain artifact (e.g., muscle or line noise, or eye movement activity) by visual inspection of their scalp topographies, time courses and activity spectra. Next, an equivalent current dipole model for each brain IC map was computed using a best fitting four-shell spherical head model in the EEGLAB *dipfit* plug-in (using *Fieldtrip* toolbox functions written by Robert Oostenveld). Components with bilaterally symmetric scalp maps were fit with two symmetrically placed but freely oriented equivalent dipoles. If the spherical forward-model scalp projection of the best-fitting single or dual-symmetric equivalent dipole model had more than 15% residual variance from the IC scalp map over all scalp electrodes, the component was omitted

from further analysis. ICs with an equivalent dipole located well outside the model brain volume were also excluded. The mean number of remaining ICs with near-dipolar scalp maps entered into the subsequent analysis was 16 per subject (± 5, std. dev.; range, 7 to 25).

Spectral analysis. For each subject, selected IC activations from emotion imagery periods were separated into 50%-overlapping 1-s time windows and then transformed into individual frequency power spectra by fast Fourier transform (FFT) with Hanning window tapering. The tapered 256-point time windows were zero-padded to 512 points to give frequency bins with 0.5-Hz spacing. Ninety-nine frequency bins between 1 and 50 Hz were selected for use and converted to log power. Mean log power at each frequency (across the roughly 2k to 10k data windows per subject) was subtracted from each single-window power spectral estimate. The resulting time series of log spectral deviations, scaled to dB units, were then concatenated, giving a matrix of size ($t, f \times c$), where t is the number of time windows, c the number of subject ICs used in the analysis, and f the number of frequency bins (99). The size of this matrix varied across subjects according to the lengths of their imagery periods and the number of their quasi-dipolar ICs used in the analysis. For each subject, this (tall) matrix was reduced to its first 15 principal dimensions by PCA, the resulting principal subspace accounting for about 10% of the original log spectral variance.

Log spectral decomposition. The dimension-reduced log spectral data were then decomposed by extended infomax ICA to find independent modulation modes of log spectral power across subsets of frequencies within all ICs. Below, we refer to the resulting modulatory factors, modes, or processes as independent modulators (IMs) that multiplicatively affect the activity spectra of one or more of the dipolar ICs separated from the recorded EEG scalp signals. The EEG model underlying this analysis is illustrated schematically in Figure 1.

[Figure 1 about here]

In Fig. 1, two IM processes are shown schematically as discs placed in the brainstem region of a cartoon head. Several neurotransmitter-labeled arousal or event valuation systems centered in the brainstem are known to modulate cortical field spectra (see Discussion). While the log spectral decomposition introduced here might possibly separate the influences of such systems on the scalp EEG, there is no guarantee that the IM processes derived statistically from the data need reflect the actions of individual physiological systems, and any such suggested linkages must be tested experimentally.

The log spectral ICA decomposition of the dimension-reduced IC spectral variability over time returns a spectral unmixing matrix. The inverse of this matrix (the spectral mixing matrix) gives the relative projection weights for each IM to each PCA dimension. These can be expanded into window time series by multiplying the ICA mixing matrix by the pseudo-inverse of the dimension-reduced PCA eigenvector matrix.

The decomposition also returns a matrix of 'templates' containing the relative modulatory effects of each IM on each IC spectrum. Multiplying the inverse ICA and pseudo-inverse PCA weight matrices with a single IM template produces a back-projected data matrix whose columns estimate the strength of IC log-power fluctuations across time windows of one IM process. Thus, IM decomposition models principal IC log power spectral fluctuations as weighted sums of IM process influences.

Exact formulation. The decomposition of spectral modulations using ICA assumes that the matrix of spectral activities, S, of each IC (*c*) in each time window is multiplicatively affected (scaled or gated) by the exponentially-weighted product of some number, *N,* of IM processes whose (template) patterns of log linear effects on each IC spectrum are given by templates comprising the rows of matrix *T*. Each of the IM templates scales power in some portions of the IC baseline spectra, *B*, the strength of these modulations given by a matrix of the scalar exponents, *W,* associated with each IM, IC, and time window. The magnitudes and polarities of these weights determine the extent to which the *N* IM templates, *T,* produce fluctuations in the IC power spectra, *S*.

$$S_{c,t} = \prod_{m=1}^{N} (T_m{}^{W_{m,t}}) \times B_c \qquad (1)$$

where $S_{c,t}$ is the power spectrum of IC c in time window t, T_m is the template of IM m in window t, $W_{m,t}$ is the frequency vector of weights for IM m in time window t, and B_c is the mean power spectrum of IC c across time windows. Taking the log of both sides gives the IC log power spectrum, S, of IC c in time window t.

$$\log S_{c,t} = \sum_{m=1}^{N} W_{m,t} \log(T_m) + \log B_c \qquad (2)$$

The log spectral deviation (D) from the mean power spectrum of c in time window t is

$$D_{c,t} = \log S_{c,t} - \log B_c = \sum_{m=1}^{N} W_{m,t} \log(T_m) \qquad (3)$$

This equation can be written to include all factors, ICs, and time windows as matrix equation

$$D = WT \qquad (4)$$

Here, D is the matrix of log spectral deviations from log spectral baseline with dimensions (windows by ICs × frequencies), the columns of matrix W, of dimensions (windows by IMs), give the time window weights, and the rows of matrix T, of dimensions (IMs by ICs × frequencies), give the templates of spectral modulation of spectral power across ICs and frequencies. For computational tractability, the height of matrix D may be reduced by PCA before ICA decomposition. The index t in equations (1)-(3) above then ranges over the retained principal temporal dimensions (here, 15).

As the baseline mean EEG spectrum resembles a power-law function, $B \propto f^{a}$, note that the spectrum, S, produced by an IM whose log template T rises slowly with frequency, $T \propto bf$ is $S = T^{w}B \propto (bf)^{w} f^{a} \propto b^{w} f^{(w+a)} \propto f^{(w+a)}$, a power-law function of frequency in which the current IM weight, w, adjusts the power-law exponent. Power law spectra appear in nonlinear systems, in particular at critical points at which they are most sensitive to external influence (Linkenkaer-Hansen et al., 2001).

Note as well the difference in the current '*WT*' ('weights × templates') decomposition (suggested by Jason Palmer, personal communication) from the alternate '*TW*' form of spectral ICA decomposition reported previously (Onton et al., 2005). In that ('*TW* ') decomposition of spectral variability in a single IC, temporal independence of the modulator time courses maximized was across time windows (as, here, in the initial ICA decomposition of the time-domain scalp data). In the present '*WT*'

decomposition, however, the independence maximized by ICA is of the IM templates across ICs and frequencies. That is, ICA here finds the most distinctive patterns of frequency modulation across spatial locations (IC combinations) and spectral frequencies whose weighted sums produce the decomposed data. In '*WT'* spectral decomposition, therefore, the estimated IM time courses themselves may be correlated and/or otherwise mutually informative.

The choice of a multiplicative model for the IM processes is mathematically convenient but also seems biologically plausible, at least within some limited range of exponential weights. In this model, biological field activity modulator processes are not assumed to add to or subtract activity from the ongoing local field spectra, but instead are modeled as scaling up or down the amplitudes of particular modes of spectral activity – whose frequency profiles and time window weights may be then estimated by ICA decomposition.

IM template clustering. To find common patterns of spectral modulations across subjects and IMs, all spectral IC template patterns whose root mean-square (RMS) amplitudes were at least 50% of the largest RMS IC template for each IM were collected for clustering. By this criterion, each IM affected between 1 and 24 ICs (mean and std. dev., 4.2 ± 3.5). Each subject contributed, on average, 63 IM templates (15 IMs × ~4.2 ICs), giving 2209 total IC frequency templates (~63 templates × 34 subjects) for clustering.

IM clustering was performed by first linearly warping IM template frequencies to equalize the mean alpha peak of the whole activity spectrum of the corresponding IC. No adjustment was performed on IM templates whose mean power spectrum did not contain a detectable alpha peak. Clustering was accomplished by first calculating the Euclidean distance between all IM template vectors and then using the Matlab '*ward*' linkage method to cluster nearby ICs (Matlab *pdist()* followed by *linkage()*. A dendrogram was constructed (Matlab *dendrogram()*) with branching set to yield 150 small but homogeneous clusters of IM templates. In these initial clusters, three categories of IM clusters were identified, primarily affecting spectral power in the alpha band (8-12 Hz), beta band (13-30 Hz), and higher frequencies respectively. IM templates in each category

were then further clustered using the same distance/linkage method, producing eight template clusters.

Results

The durations of the 510 recorded emotion periods (15 emotions × 34 subjects) were between 43 sec and 12 min (on average, 218 ± 94 sec) during experimental sessions of about 80 minutes.

[Figure 2 about here]

Representative Results. Figure 2 shows effects of seven IMs on 11 (of 20) ICs used in the analysis of one subject's data. Each figure row represents one IM and each column one IC. Note that IM12 clearly modulates only IC9, while other IMs clearly co-modulate the spectra of 3-7 ICs. Like the IMs of other subjects, most of the non-negligible spectral templates for each IM are highly correlated, though the ICA decomposition was in no way constrained to produce this result. (Note, however, that the activation template of IM9 on IC22 also includes a weak negative effect around 10 Hz not apparent in its larger effects on, for example, IC19; the significance of such anomalies is not investigated here). The left column of Fig. 2 shows the distributions of time window weights for each IM; all are unimodal and bivalent, with varying skew and kurtosis.

Fig. 3 depicts the maximal effects of five IMs on nine ICs from Fig. 2. The back-projections of the most positively-weighted time window for each IM (colored traces) are added to their respective baseline mean power spectra (black traces). The superposition of IMs in each panel emphasizes the frequency specificity and unique modulation patterns of each IM on the selected IC spectra. For example, IM1 and IM4 modulate the upper and lower edges of alpha-band power for IC1 and IC8 (lower central panels). Note that the IM3 beta-band (15-20 Hz) modulation of IC1 (center panel) does not affect power at the alpha-harmonic beat band peak near 20 Hz, which is controlled by IM1 and IM4. However, the IM3 beta modulation is near the harmonic of the mean IC15 alpha peak, illustrated by the beta peak of IM5 (right middle panel), which produces an alpha

band modulation at a slightly slower frequency than the alpha-band peak frequencies of IM1 and IM4.

[Figure 3 about here]

The upper limits of the grey shaded regions in Fig. 3 show, for each IC, the upper $99^{\underline{th}}$ power percentiles at each frequency. The limits of the PCA-reduced data are shown in dark grey. For some ICs (IC1 and IC8), the maximal contributions of the illustrated IMs account for the extremes of the darker grey area, but for other ICs (IC18), the variability of the PCA-reduced data is accounted for by other IMs (not shown).

[Figure 4 about here]

Figure 4 illustrates the variability in time-domain and spectral activity of one IC accounting for left-central and frontal-midline scalp mu-rhythm activity. Two modulators (IM3 and IM4) modulate IC13 power in the alpha range, one maximally near 10 Hz and the other near 12 Hz. The mean IC alpha-band peak, across all time windows, falls between the alpha peaks of these modulators (i.e., near 11 Hz). In Fig. 4, several time windows are selected as highly weighted on IM3, IM4 or both (B, scatter plot), and the phase-aligned IC activity time courses centered on these highly weighted windows (D) are overplotted. In both sets of time windows, the IC activity has a non-sinusoidal, spindle-like pattern with sharp triangular peaks and broad, blunted troughs, hence the designation '*μ rhythm'*. This wave shape produces the harmonically coupled alpha and beta band peaks in the IC window spectra (C). Thus, the two IMs index regulation of periodic but non-sinusoidal mu-activity patterns at two different alpha band frequencies.

IM Clusters. Cluster analysis (see Methods) was used to derive eight IM clusters with different frequency characteristics and patterns of spatial effects. The eight identified clusters could be grouped into three classes of IMs most notably affecting alpha, beta, and higher frequency activities, respectively.

[Figure 5 about here]

Alpha-band modulators. The class of IMs predominantly affecting alpha-band power comprised three IM clusters (Fig. 5). The first cluster (Fig. 5A) predominantly modulated the IC mean peak alpha-band frequency (1×) and its harmonics (2× and 3×), while the other two alpha-band clusters had maximal effects on alpha-band activity 1-2 Hz below (B) or above (C) the mean IC alpha-band peak and, again, at its harmonics. The sample IMs shown on the right of Fig. 5 demonstrate the typically similar pattern of frequency effects of these IMs on all the affected ICs.

Balls in the central panels of Fig. 5 represent the positions of equivalent dipole models for affected ICs, their color varying according to the sign and root mean-square (RMS) strength of their IM template, relative to its most-strongly modulated IC. Black balls represent equivalent dipoles of ICs solely affected by an IM, without IC co-modulates, while green lines connect ICs modulated by the same IM. Blue spheres indicate that the effect of the IM on the IC spectrum is opposite to its effect on the maximally-affected IC, while dipoles shown by red or warm-color balls represent ICs co-modulated by the IM in the same direction as the maximally-affected IC.

ICs affected by the three alpha-band IM clusters were densely distributed across similar occipital, parietal and somatomotor areas, but were significantly absent from frontal cortex. Fig. S1 (second row) in Supplement A shows the spatial distribution of their combined density difference from similar-sized density distributions drawn at random from all the ICs used in the analysis (first row). In the ‘at-peak’ alpha-band cluster, 46% of IMs (53 of 116) affected power at a single IC, while 78% of the ‘off-peak’ alpha-band cluster IMs (262 of 335) co-modulated the maximally independent activities of at least two ICs. More often than expected by chance (Fig. S2), the off-peak cluster ICs were located near bilaterally across the mid-sagittal sulcus, and more of the off-peak cluster ICs were best modeled by bilateral equivalent dipole pairs ($p << 0.01$ by permutation testing). The at-peak cluster had a similar but weaker trend ($p = 0.055$).

[Figure 6 about here]

Beta-band modulators. Two clusters of beta-band IMs primarily affecting low beta band (~13-25 Hz) and high beta band (or low gamma band) (~25-35 Hz) activity, respectively. High-beta band IMs were drawn from only 15 (44%) of the 34 subjects, while low-beta band modulators were recovered from 26 subjects (76%). The sample IMs shown in Fig. 6 (right) demonstrate the typically similar pattern of frequency effects of these IMs on the affected ICs. Density of ICs affected by low-beta band IMs was high in portions of left central and in right frontal cortex, and was low in central medial brain areas (Fig. S1, third row). For this cluster also, bilateral left-right dipole pairs were co-modulated more often than by chance and co-modulated dipole pair distance featured nearby dipoles (Fig. S3).

High-beta band IMs were unexpectedly dense in central somatomotor regions bilaterally, and were absent from medial occipital cortex (Figs. 6A, S1). Of the beta-band cluster IMs, only 11% were 'solo' IMs (15/137 low-beta; 7/55 high-beta) without above-threshold effects on other ICs.

[Figure 7 about here]

Broadband modulators. Three clusters of IMs modulated power across a broad frequency range, with strongest relative effects in the gamma band (above 30 Hz). The first such cluster (Fig. 7A) affected the global balance between high-frequency and low-frequency power in many or all of the IC processes included in the analysis, with a mean fulcrum frequency near 25 Hz.

A second broadband IM cluster (Fig 7B) selectively modulated power of some ICs at all frequencies above 20 Hz, with smoothly increasing effect at higher frequencies, and including effects of opposite sign, as in the example shown on the right. Essentially, IM templates including positive and negative template effects shifted the spatial balance of high-frequency EEG power across the affected IC subset. However, detailed inspection of the locations of IMs co-modulated with opposite signs revealed no simple

spatial pattern in these differences. Fully 95% of cluster IMs (164 of 172) affected more than one IC. The distribution of affected ICs was significantly dense in left somatomotor and right temporal cortex and near the frontal pole, and sparse in superior medial posterior cortex (Fig. S1). This cluster also included significantly more near-bilaterally situated co-modulated IC dipole pairs than random selection, and more closely situated co-modulated IC pairs (Fig. S3).

A third broadband IM cluster modulated broadband power smoothly across all analysis frequencies above 5-10 Hz, but only for a single IC (Fig. 7C). A significant density of cluster IM dipoles was situated in orbitofrontal cortex (Fig. S1), and a significant void in medial occipital and centromedial cortex.

Broadband IM frequency range. Fig. 7 suggests that the peak frequency of the broadband IM effects was well above the 50-Hz limit of our analysis. High gamma activity between 70 Hz and 200 Hz has recently been shown to be positively correlated with increased local energy uptake by functional magnetic resonance imaging (fMRI) and with active local sensory processing by electrocorticography (Crone et al., 1998; Sinai et al., 2005; Canolty et al., 2006). To explore the upper frequency limits of the broadband IM templates we conducted trial decompositions for a few subjects including the full frequency range (1-125 Hz) allowed by our sampling rate (256 Hz). Results (Fig. S5) included some broadband IM templates that peaked between 50 and 125 Hz, while many other broadband IM templates increased to a plateau beginning at 50-80 Hz, or still continued to increase at the 125 Hz cutoff, strongly suggesting they produced largest (dB) effects at still higher frequencies.

Independence of broadband cortical and electromyographic modulations. Because broadband power fluctuations at frequencies above about 20 Hz are also characteristic of electromyographic (EMG) activity of scalp muscles, it might be suggested that the observed broadband IMs affecting cortical ICs may have simply captured muscle activity leaking into the spatially filtered cortical IC signals. To test this possibility, we performed separate control decompositions on several subjects that included ICs predominantly accounting for cortical EEG, scalp electromyographic (EMG), and electro-ocular (EOG)

activities (not shown), respectively. As expected, some resulting IMs clearly modulated (~20 Hz -100+ Hz) EMG activity in ICs accounting predominantly for muscle artifact (Fig. S5, left side). However, these IMs had no effects on ICs accounting predominantly for cortical EEG activity. Conversely, broadband IMs that modulated activity of cortical ICs (Fig. S5, right side) did not co-modulate activity of muscle or eye movement ICs, with one exception: Inferior-frontal solo broadband cluster IMs (Fig. 7C) were sometimes found to also modulate power at high frequencies in ICs predominantly accounting for eye movement artifacts.

Discussion

Here we model spectral fluctuations of independent components from high-density EEG data as the actions of independently regulated modulator processes with frequency-selective multiplicative effects on independent component process activities, and report three main classes of spectral modulation patterns. Physiological processes that may produce these patterns include several brain systems regulating brain and behavioral arousal and/or valuation judgments of stimulus and other events via the release by midbrain or brainstem neurons of modulatory neurotransmitters – dopamine (DA), acetylcholine (ACh), norepinephrine (NE), serotonin, etc. – through their extensive cortical and thalamic projections (Robbins, 1997; Bardo, 1998). For example, application of the muscarinic agonist carbachol to CA3 hippocampal slices has been shown to induce delta, theta, and/or gamma band oscillations, depending on its concentration (Fellous and Sejnowski, 2000). However, any physiological model of the recovered spectral modulations must be evaluated experimentally.

Alpha-band modulators. Our results demonstrate clearly that specificalpha -band EEG activities are mainly generated by non-sinusoidal spindle-wave processes that contribute harmonically linked (1×, 2×, 3×) frequencies to EEG spectra, and that IC (and scalp EEG) alpha-band activities are the product of multiple spindle-generating processes, often with slightly different periods. The unforced appearance of maximal alpha-band IM effects at exact harmonics (Figs. 2-3), and the time-domain appearance of activities in

time windows highly-weighted on single alpha-peaked IMs (Fig. 4), strongly imply that both posterior and central scalp alpha activities recovered from these data reflect the waxing and waning of asymmetrical alpha-band spindles at periodicities near 100 ms. While coupling between alpha and beta power spectral peaks is prominent for centrolateral mu-rhythm processes (Gaarder and Speck, 1967; Jurgens et al., 1995; Pfurtscheller et al., 1997), its appearance here in posterior eyes-closed alpha activity is more novel.

A recent related analysis of spectral modulations in frontal midline ICs during a working memory experiment also showed that the frontal midline theta rhythm near 6 Hz, associated with concentration, also has an asymmetric spindle waveform and a (2×) harmonic spectral peak (Onton et al., 2005). Thus, both posterior and centrolateral alpha-band and frontal midline theta-band rhythms are non-sinusoidal spindle rhythms, despite marked differences in cortical locations, frequencies, and contexts in which they appear.

Note that nearly no equivalent dipole models of IC processes affected by the alpha-band IMs were located in frontal lobe (Figs. 5, S2), in contrast to interpretation of differences in alpha-band power between left and right frontal scalp sites, linked to emotion differences, as reflecting frontal brain processes (Schaffer et al., 1983). Task differences might explain this discrepancy; else, such effects might not reflect alpha-band activity generated in frontal cortex or might not be specifically associated with alpha-band modulation.

Our alpha-band results are not inconsistent with reported associations between alpha-band frequencies and cognitive processes (Vogt et al., 1998). In these studies, alpha-band effects were assigned to ‘upper’ and ‘lower’ alpha bands relative to a posited peak mean individual subject alpha frequency (IAF) averaged across posterior *scalp channels* (Klimesch et al., 1998). Our results, by contrast, revealed three clusters of alpha IMs at, below, and above the *individual IC* peak mean frequency – an important difference (see Fig. 2). These results show that only a multiple spatiotemporal source model, such as the ICA-based model we used here, can adequately account for the spectral and spatial complexity of alpha-band scalp activity.

Our model also differs from those positing alpha-band power fluctuations to be dominated by a non-separable, nonlinear dynamic mechanism that produces modulation

time series that are self-similar over a wide range of time scales (Linkenkaer-Hansen et al., 2001). Though in their simplest form such models ignore the spatial complexity of alpha-band activity and its clear reactivity to external events, it could be of interest to apply such time-series embedding analyses to IC and IM time series.

Physiology. Several neuromodulators (including ACh and GABA) are known to affect alpha-band power (Lukatch and MacIver, 1997; Bao and Wu, 2003). ACh plays an important role in regulating attention related to alpha-band power modulation (Worden et al., 2000), and also plays a role in memory as shown by animal ACh deprivation experiments (Arendt, 1994). In presumably ACh-deprived early Alzheimer's dementia patients, the peak mean alpha-band frequency decreases slightly (Coben et al., 1983), while ACh-agonist nicotine increases the resting alpha-band frequency (Kadoya et al., 1994; Lindgren et al., 1999). These reports suggest possible ACh involvement in the alpha-band IM processes.

Beta-band modulators. Lower and higher beta-band IMs (Fig. 6) were largely free of harmonic structure, consistent with long-reported observations of beta band activities independent of lower frequency rhythms (Roopun et al., 2006). Some beta-band activity is associated with DA as it is disrupted by nigro-striatal DA projection damage in Parkinson's disease (Pezard et al., 2001; Williams et al., 2002), D2 receptor antagonists (Dimpfel et al., 1992), and increased by acute cocaine administration (Herning et al., 1985). ACh has also been shown to increase neuronal firing frequency in thalamic slice preparations (McCormick, 1992). The prevalence, as shown in Fig. S1, of high-beta band activity along the sensorimotor strip has long been noted (Jasper, 1949; Crone et al., 1998).

Broadband modulators. Although gamma-band phenomena observed *in vivo* are often reported to have a wide-band character, both the width and smoothness of the broadband IM frequency templates (Fig. 7) is striking, suggesting global, distributed, and region-specific changes in cortical excitation. Together, they suggest the possibility that previous analyses of gamma-band effects, both on the scalp and in the cortex, may have missed

their true spectral extent through masking by other modulator processes, especially at lower frequencies, and by other activities including muscle artifacts at higher frequencies. Else, possibly IM analysis of data collected during performance of other tasks might reveal narrower gamma-band effects.

Global high/low cluster. The frequency profile of the global high/low IM cluster (Fig. 7A) is generally consistent with changes in behavioral arousal (Makeig and Jung, 1996). ACh is associated with behavioral arousal through its effects on thalamus (Steriade et al., 1982), and its extensive projections from the basal forebrain (Stewart et al., 1985) inhibit low-frequency and promote high-frequency cortical activity (Stewart et al., 1984; Herculano-Houzel et al., 1999). NE projections from the locus coeruleus (LC) are also widespread throughout cortex (Jones et al., 1977), and LC stimulation in both awake monkeys (Swick et al., 1994) and anesthetized rats (Berridge and Foote, 1991; Brown et al., 2005) also reduces low-frequency and increases high-frequency local field activity, both in frontal cortex and thalamus (Pinault and Deschenes, 1992). The correlation between local field power and BOLD signal in auditory cortex has a similar frequency profile that further associates cortical high-frequency versus low-frequency balance with arousal (Mukamel et al., 2005).

Broadband clusters. Rather than being confined to a particular band, the two broadband IM clusters (Figs. 7B and 7C) scale a wide portion of the EEG spectrum with a dB weighting that increases smoothly with frequency. As noted in Methods, slowly increasing IM templates affect the power-law fall-off of the affected IC spectra. Power-law scaling of local field events has been observed in isolated visual cortex (Beggs and Plenz, 2003), though Bedard et al. argue that 1/f scaling of local field and EEG signals may also be produced simply by capacitive filtering effects of cell membranes in neuropile (Bedard et al., 2006). The possible plateau in broadband cluster templates above 40 Hz (Fig. 7B-C) was confirmed in several trial decompositions with frequencies between 1 and 125 Hz in which broadband IM template effects were sometimes near-constant between ~50 Hz and 125 Hz (Fig. S5).

Solo broadband IMs. This IM cluster demonstrates that ICA applied to scalp data can spatially separate gamma-band phenomena. Conceivably, the cluster of solo broadband IMs equivalent dipoles in medial sub-genual cortex (Figs. 7C, S1), strongly connected to amygdala and limbic influences, might reflect participants' active emotional control during these experiments (Bush et al., 2000; Winston et al., 2003; Koenigs and Tranel, 2007), while the relative lateral occipital solo broadband IM densities (Fig. S1) might support their use of visual imagery (Kosslyn et al., 1995; Pietrini et al., 2004). Note that, unlike in working memory experiments (Onton et al., 2005), in the current experiments no IC density or IM cluster appeared in or near dorsal anterior cingulate cortex (Fig. S1).

Conclusions. Together, these results demonstrate that the dynamic character of locally synchronous cortical field potentials that produce scalp EEG activity exhibits distinct modes of concurrent variation with several new or under-appreciated features: (a) the dominance of non-sinusoidal alpha-band spindles in both centrolateral and posterior cortex; (b) the appearance of alpha spindle IMs with distinct alpha-band peak frequencies in the same ICs; (c) the clear separation of alpha-harmonic beta modulation from uniquely beta-band modulators, and (d) the three types of markedly broadband modulators, whose presence and full frequency span may have been masked in previous EEG analyses based on pre-defined frequency bins or bands by the complexity of spectral dynamics. The generality of the results reported here must be evaluated across subject task and analysis parameters. Exploring the relationship of the recovered IM modes to actions of known neuromodulatory systems may also be of interest.

Acknowledgments

This work was supported by a gift from The Swartz Foundation (Old Field, NY). Dr. Makeig also receives support from NIMH (R01 NS074293), NSF (IIS-0613595), and DARPA (NBCH1060010). The authors thank Jason Palmer, Lars Kai Hansen, Jack Cowan, and Erik Edwards for helpful discussions, and Stefan Debener for suggestions on the manuscript.

Citations

Andrew C, Pfurtscheller G (1997) On the existence of different alpha band rhythms in the hand area of man. Neurosci Lett 222:103-106.

Arendt T (1994) Impairment in memory function and neurodegenerative changes in the cholinergic basal forebrain system induced by chronic intake of ethanol. J Neural Transm Suppl 44:173-187.

Bao W, Wu JY (2003) Propagating wave and irregular dynamics: spatiotemporal patterns of cholinergic theta oscillations in neocortex in vitro. J Neurophysiol 90:333-341.

Bardo MT (1998) Neuropharmacological mechanisms of drug reward: beyond dopamine in the nucleus accumbens. Crit Rev Neurobiol 12:37-67.

Bedard C, Kroger H, Destexhe A (2006) Does the 1/f frequency scaling of brain signals reflect self-organized critical states? Phys Rev Lett 97:118102.

Beggs JM, Plenz D (2003) Neuronal avalanches in neocortical circuits. J Neurosci 23:11167-11177.

Berridge CW, Foote SL (1991) Effects of locus coeruleus activation on electroencephalographic activity in neocortex and hippocampus. J Neurosci 11:3135-3145.

Brown RA, Walling SG, Milway JS, Harley CW (2005) Locus ceruleus activation suppresses feedforward interneurons and reduces beta-gamma electroencephalogram frequencies while it enhances theta frequencies in rat dentate gyrus. J Neurosci 25:1985-1991.

Bush G, Luu P, Posner MI (2000) Cognitive and emotional influences in anterior cingulate cortex. Trends Cogn Sci 4:215-222.

Canolty RT, Edwards E, Dalal SS, Soltani M, Nagarajan SS, Kirsch HE, Berger MS, Barbaro NM, Knight RT (2006) High gamma power is phase-locked to theta oscillations in human neocortex. Science 313:1626-1628.

Cantero JL, Atienza M, Madsen JR, Stickgold R (2004) Gamma EEG dynamics in neocortex and hippocampus during human wakefulness and sleep. Neuroimage 22:1271-1280.

Coben LA, Danziger WL, Berg L (1983) Frequency analysis of the resting awake EEG in mild senile dementia of Alzheimer type. Electroencephalogr Clin Neurophysiol 55:372-380.

Crone NE, Miglioretti DL, Gordon B, Lesser RP (1998) Functional mapping of human sensorimotor cortex with electrocorticographic spectral analysis. II. Event-related synchronization in the gamma band. Brain 121 (Pt 12):2301-2315.

Delorme A, Makeig, S. (2004) EEGLAB: an open source toolbox for analysis of single-trial EEG dynamics. Journal of Neuroscience Methods 134:9-21.

Delorme A, Sejnowski, T., Makeig, S. (In press) Improved rejection of artifacts from EEG data using high-order statistics and independent component analysis. NeuroImage.

Dimpfel W, Spuler M, Wessel K (1992) Different neuroleptics show common dose and time dependent effects in quantitative field potential analysis in freely moving rats. Psychopharmacology (Berl) 107:195-202.

Fellous JM, Sejnowski TJ (2000) Cholinergic induction of oscillations in the hippocampal slice in the slow (0.5-2 Hz), theta (5-12 Hz), and gamma (35-70 Hz) bands. Hippocampus 10:187-197.

Freeman WJ (2004) Origin, structure, and role of background EEG activity. Part 1. Analytic amplitude. Clin Neurophysiol 115:2077-2088.

Fries P, Neuenschwander S, Engel AK, Goebel R, Singer W (2001) Rapid feature selective neuronal synchronization through correlated latency shifting. Nat Neurosci 4:194-200.

Gaarder K, Speck LB (1967) The quasi-harmonic relations of alpha and beta peaks in the power spectrum. Brain Res 4:110-112.

Herculano-Houzel S, Munk MH, Neuenschwander S, Singer W (1999) Precisely synchronized oscillatory firing patterns require electroencephalographic activation. J Neurosci 19:3992-4010.

Herning RI, Jones RT, Hooker WD, Mendelson J, Blackwell L (1985) Cocaine increases EEG beta: a replication and extension of Hans Berger's historic experiments. Electroencephalogr Clin Neurophysiol 60:470-477.

Jasper H, Penfield, W (1949) Electrocorticograms in man: Effect of voluntary movement upon the electrical activity of the precentral gyrus. Europ Arch Psychiatr Clin Neurosci 183:163-174.

Jones BE, Halaris AE, McIlhany M, Moore RY (1977) Ascending projections of the locus coeruleus in the rat. I. Axonal transport in central noradrenaline neurons. Brain Res 127:1-21.

Jung T-P, Makeig, S., McKeown, MJ., Bell, AJ., Lee, T-W., Sejnowski, TJ. (2001) Imaging brain dynamics using independent component analysis. Proceedings of the IEEE 89:1107-1122.

Jurgens E, Rosler F, Henninghausen E, Heil M (1995) Stimulus-induced gamma oscillations: harmonics of alpha activity? Neuroreport 6:813-816.

Jurkiewicz MT, Gaetz WC, Bostan AC, Cheyne D (2006) Post-movement beta rebound is generated in motor cortex: evidence from neuromagnetic recordings. Neuroimage 32:1281-1289.

Kadoya C, Domino EF, Matsuoka S (1994) Relationship of electroencephalographic and cardiovascular changes to plasma nicotine levels in tobacco smokers. Clin Pharmacol Ther 55:370-377.

Klimesch W, Doppelmayr M, Pachinger T, Russegger H (1997) Event-related desynchronization in the alpha band and the processing of semantic information. Brain Res Cogn Brain Res 6:83-94.

Klimesch W, Doppelmayr M, Russegger H, Pachinger T, Schwaiger J (1998) Induced alpha band power changes in the human EEG and attention. Neurosci Lett 244:73-76.

Koenigs M, Tranel D (2007) Irrational economic decision-making after ventromedial prefrontal damage: evidence from the Ultimatum Game. J Neurosci 27:951-956.

Kosslyn SM, Thompson WL, Kim IJ, Alpert NM (1995) Topographical representations of mental images in primary visual cortex. Nature 378:496-498.

Lee TW, Girolami M, Sejnowski TJ (1999) Independent component analysis using an extended infomax algorithm for mixed subgaussian and supergaussian sources. Neural Comput 11:417-441.

Leocani L, Toro C, Manganotti P, Zhuang P, Hallett M (1997) Event-related coherence and event-related desynchronization/synchronization in the 10 Hz and 20 Hz EEG during self-paced movements. Electroencephalogr Clin Neurophysiol 104:199-206.

Lindgren M, Molander L, Verbaan C, Lunell E, Rosen I (1999) Electroencephalographic effects of intravenous nicotine--a dose-response study. Psychopharmacology (Berl) 145:342-350.

Linkenkaer-Hansen K, Nikouline VV, Palva JM, Ilmoniemi RJ (2001) Long-range temporal correlations and scaling behavior in human brain oscillations. J Neurosci 21:1370-1377.

Lukatch HS, MacIver MB (1997) Physiology, pharmacology, and topography of cholinergic neocortical oscillations in vitro. J Neurophysiol 77:2427-2445.

Makeig S, Jung TP (1996) Tonic, phasic, and transient EEG correlates of auditory awareness in drowsiness. Brain Res Cogn Brain Res 4:15-25.

Makeig S, Debener S, Onton J, Delorme A (2004) Mining event-related brain dynamics. Trends Cogn Sci 8:204-210.

Makeig S, Jung TP, Bell AJ, Ghahremani D, Sejnowski TJ (1997) Blind separation of auditory event-related brain responses into independent components. Proc Natl Acad Sci U S A 94:10979-10984.

Makeig S, Westerfield M, Jung TP, Enghoff S, Townsend J, Courchesne E, Sejnowski TJ (2002) Dynamic brain sources of visual evoked responses. Science 295:690-694.

Makeig S, Bell, AJ.,Jung, TP., Sejnowski, TJ. (1996) Independent component analysis of electroencephalographic data. Advances in Neural Information Processing Systems 8:145-151.

McCormick DA (1992) Cellular mechanisms underlying cholinergic and noradrenergic modulation of neuronal firing mode in the cat and guinea pig dorsal lateral geniculate nucleus. J Neurosci 12:278-289.

Mukamel R, Gelbard H, Arieli A, Hasson U, Fried I, Malach R (2005) Coupling between neuronal firing, field potentials, and FMRI in human auditory cortex. Science 309:951-954.

Onton J, Makeig S (2006) Chapter 7 Information-based modeling of event-related brain dynamics. Prog Brain Res 159:99-120.

Onton J, Delorme A, Makeig S (2005) Frontal midline EEG dynamics during working memory. Neuroimage 27:341-356.

Pfurtscheller G, Neuper C, Andrew C, Edlinger G (1997) Foot and hand area mu rhythms. Int J Psychophysiol 26:121-135.

Pietrini P, Furey ML, Ricciardi E, Gobbini MI, Wu WH, Cohen L, Guazzelli M, Haxby JV (2004) Beyond sensory images: Object-based representation in the human ventral pathway. Proc Natl Acad Sci U S A 101:5658-5663.

Pinault D, Deschenes M (1992) Control of 40-Hz firing of reticular thalamic cells by neurotransmitters. Neuroscience 51:259-268.

Robbins TW (1997) Arousal systems and attentional processes. Biol Psychol 45:57-71.

Roopun AK, Middleton SJ, Cunningham MO, LeBeau FE, Bibbig A, Whittington MA, Traub RD (2006) A beta2-frequency (20-30 Hz) oscillation in nonsynaptic networks of somatosensory cortex. Proc Natl Acad Sci U S A 103:15646-15650.

Schaffer CE, Davidson RJ, Saron C (1983) Frontal and parietal electroencephalogram asymmetry in depressed and nondepressed subjects. Biol Psychiatry 18:753-762.

Sinai A, Bowers CW, Crainiceanu CM, Boatman D, Gordon B, Lesser RP, Lenz FA, Crone NE (2005) Electrocorticographic high gamma activity versus electrical cortical stimulation mapping of naming. Brain 128:1556-1570.

Singer W, Gray CM (1995) Visual feature integration and the temporal correlation hypothesis. Annu Rev Neurosci 18:555-586.

Steriade M, Oakson G, Ropert N (1982) Firing rates and patterns of midbrain reticular neurons during steady and transitional states of the sleep-waking cycle. Exp Brain Res 46:37-51.

Stewart DJ, MacFabe DF, Vanderwolf CH (1984) Cholinergic activation of the electrocorticogram: role of the substantia innominata and effects of atropine and quinuclidinyl benzilate. Brain Res 322:219-232.

Stewart DJ, MacFabe DF, Leung LW (1985) Topographical projection of cholinergic neurons in the basal forebrain to the cingulate cortex in the rat. Brain Res 358:404-407.

Swick D, Pineda JA, Schacher S, Foote SL (1994) Locus coeruleus neuronal activity in awake monkeys: relationship to auditory P300-like potentials and spontaneous EEG. Exp Brain Res 101:86-92.

Vogt F, Klimesch W, Doppelmayr M (1998) High-frequency components in the alpha band and memory performance. J Clin Neurophysiol 15:167-172.

Winston JS, O'Doherty J, Dolan RJ (2003) Common and distinct neural responses during direct and incidental processing of multiple facial emotions. Neuroimage 20:84-97.

Worden MS, Foxe JJ, Wang N, Simpson GV (2000) Anticipatory biasing of visuospatial attention indexed by retinotopically specific alpha-band electroencephalography increases over occipital cortex. J Neurosci 20:RC63.

Wrobel A (2000) Beta activity: a carrier for visual attention. Acta Neurobiol Exp (Wars) 60:247-260.

Figure legends:

Figure 1. Independent spectral modulators of scalp EEG signals. *Independent component analysis (ICA), applied to EEG data recorded at a large number of scalp electrodes, (a) identifies temporally distinct (independent) signals generated by partial synchronization of local field potentials within cortical patches (b) and summing (Σ) in different linear combinations at each electrode depending on the distance and orientation of each cortical patch from the scalp (a) and reference electrode (c). The spectra of resulting cortical independent components (ICs) monotonically decrease with frequency, on average, but exhibit large and frequent variations across time. These spectral modulations may be modeled as exponentially weighted influences of several near-independent modulator (IM) processes (d) that independently modulate or scale (Π) the activity spectra of one or more independent component (IC) signals. On converting the IC spectra to log power, combined IM influences on IC spectra are converted to log-linear weighted sums of IM influences, allowing a second linear ICA decomposition, applied to the IC log power spectra, to separate the effects of the individual IM processes (d) across EEG frequencies and IC sources (b).*

Figure 2. Representative independent modulation templates from one subject. *IM window weights and frequency templates derived by multiplying the series of spectral deviations from the mean in each 1-s overlapping time window with the PCA/ICA unmixing matrix. Each row represents a computed IM, and each column an IC. The figure shows the relative effects of 7 of 15 extracted IMs for this subject on the log power spectra of 11 ICs out of the 20 ICs used in the analysis. The top row shows the IC scalp maps, and the leftmost column, the IM window weight histograms. Most IMs modulated the spectra of several ICs (colored squares), except IM12, which modulated power at higher frequencies for IC9 only.*

Figure 3. Maximal IM effects on IC power spectra. *The maximal positive effects of five IMs (from Fig. 2) on the power spectra of nine ICs (colored traces), computed by back-projecting the highest positive time window weight for each IM and adding back the IC mean log-power spectrum (black traces). The upper borders of the grey areas show the (99^{th}-percentile) maxima of raw power at each frequency, both in the entire IC data*

(lighter grey) and in the dimension-reduced data decomposed by ICA (darker grey). Note the various (here, positive) effects of the IMs on the IC spectra.

Figure 4. Multiple modulations of IC alpha band activity. ***A.*** *Maximal spectral modulations (as in Fig. 3) for two alpha band modulators (IM3 and IM4) acting on a left somatomotor component (IC13) accounting for mu-rhythm activity across left parietal and frontal midline scalp (see map, B).* ***B.*** *Upper panel: Map of the IC13 scalp projection. Blue and yellow areas receive projections with opposite sign. Lower panel: Scatter plot of IM3 versus IM4 window weights. Red and light blue dots group time windows with dominant IM3 and IM4 weighting, respectively. Lavender dots show time windows positively weighted for both modulators.* ***C.*** *Colored traces show the IC13 power spectra for the selected time windows (from B). Black traces plot the means of the selected window spectra. Note the variations in peak alpha frequency between 10 Hz and 12 Hz, here modeled as reflecting the influences of IM3 and IM4.* ***D.*** *Light blue and red traces show 3 s of IC13 activity centered on the midpoints of the selected time windows (see B and C) and then aligned to their central upward-going central peaks. Black traces show the mean phase-alignedactivations. The vertical dotted black line indicates the center of phase alignment and the slanted dotted lines, the* $\pm 10^{th}$ *local maxima in each mean waveform. The mean and single-trial activity waveforms are not sinusoidal, but rather are composed of sharp upward-going peaks and broad, blunted troughs, like the Greek letter mu (*μ*).*

Figure 5. Alpha-band IM clusters. *IMs for the 34 subjects were clustered based on similarities in power modulation templates. IM template frequency axes were linearly warped to align the respective IC mean alpha-band peak frequency to 1× (10 Hz). Red traces are clustered frequency-adjusted IM templates, and black traces their means. Mean MRI images show the 3-D distribution of equivalent dipole localizations of ICs contributing one or more IM templates to the cluster. Black balls are clustered IMs without co-modulates. Green lines connect co-modulated ICs (i.e., ICs with clustered templates belonging to the same IM). Warm-color balls indicate IC dipoles co-modulated with the same sign as the maximally modulated IC dipole; cool-color balls dipoles of ICs co-modulated with opposite sign. The three alpha-band IM clusters*

affected IC activity either at, below, or above the mean IC alpha peak frequency, respectively.

Figure 6. Beta-band IM clusters. *Two clusters of beta-band modulators maximally affecting low beta (13-25 Hz) and high beta (25-35 Hz) activities respectively. (Left panels) Clustered IM templates (blue traces), and their means (black traces). (Center panels) 3-D distribution of equivalent dipole locations, as in Fig. 5, for ICs modulated by clustered IMs. (Right panels) Sample IM templates for each cluster.*

Figure 7. Broadband IM clusters. *(Left panels) Broadband IM templates (green traces) and their means (black traces). (Center panels) Equivalent dipole distributions of modulated ICs (as in Fig. 5). (Right panels) Sample IM templates for each cluster.* ***A.*** *Global high/low cluster of IMs adjusting the ratio of high-frequency versus low-frequency power in all cortical ICs, with a mean frequency fulcrum near 25 Hz.* ***B.*** *Cluster of IMs that selectively co-modulated and/or spatially redistributed broadband power across several (but not all) IC, with stronger effects at higher frequencies.* ***C.*** *Cluster of IMs that increased or decreased broadband power above 5-10 Hz, and particularly above 30 Hz, in a single IC process.*

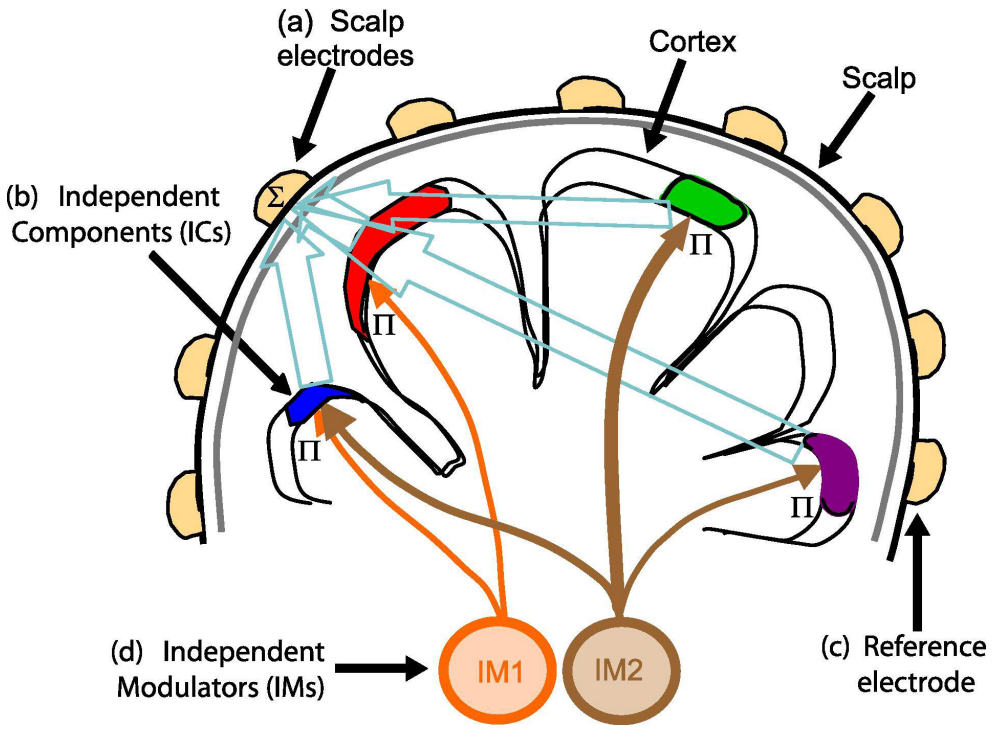

Figure 1. Independent spectral modulators of scalp EEG signals. Independent component analysis (ICA), applied to EEG data recorded at a large number of scalp electrodes, (a) identifies temporally distinct (independent) signals generated by partial synchronization of local field potentials within cortical patches (b) and summing (Σ) in different linear combinations at each electrode depending on the distance and orientation of each cortical patch from the scalp (a) and reference electrode (c). The spectra of resulting cortical independent components (ICs) monotonically decrease with frequency, on average, but exhibit large and frequent variations across time. These spectral modulations may be modeled as exponentially weighted influences of several near-independent modulator (IM) processes (d) that independently modulate or scale (Π) the activity spectra of one or more independent component (IC) signals. On converting the IC spectra to log power, combined IM influences on IC spectra are converted to log-linear weighted sums of IM influences, allowing a second linear ICA decomposition, applied to the IC log power spectra, to separate the effects of the individual IM processes (d) across EEG frequencies and IC sources (b).

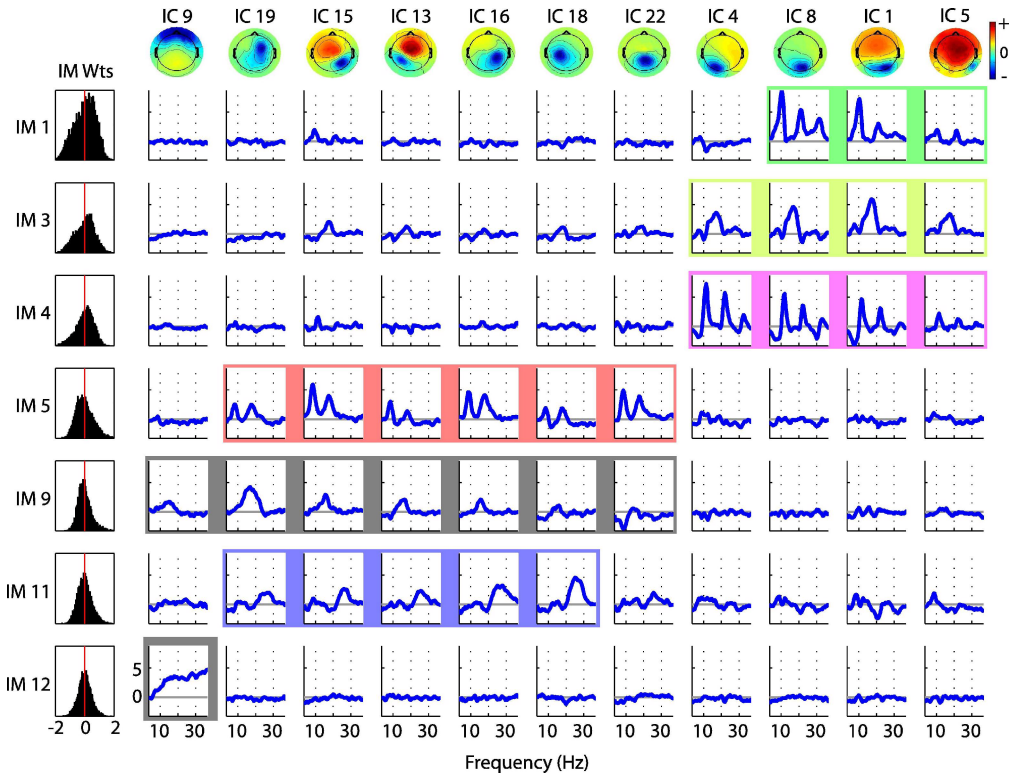

Figure 2. Representative independent modulation templates from one subject. IM window weights and frequency templates derived by multiplying the series of spectral deviations from the mean in each 1-s overlapping time window with the PCA/ICA unmixing matrix. Each row represents a computed IM, and each column an IC. The figure shows the relative effects of 7 of 15 extracted IMs for this subject on the log power spectra of 11 ICs out of the 20 ICs used in the analysis. The top row shows the IC scalp maps, and the leftmost column, the IM window weight histograms. Most IMs modulated the spectra of several ICs (colored squares), except IM12, which modulated power at higher frequencies for IC9 only.

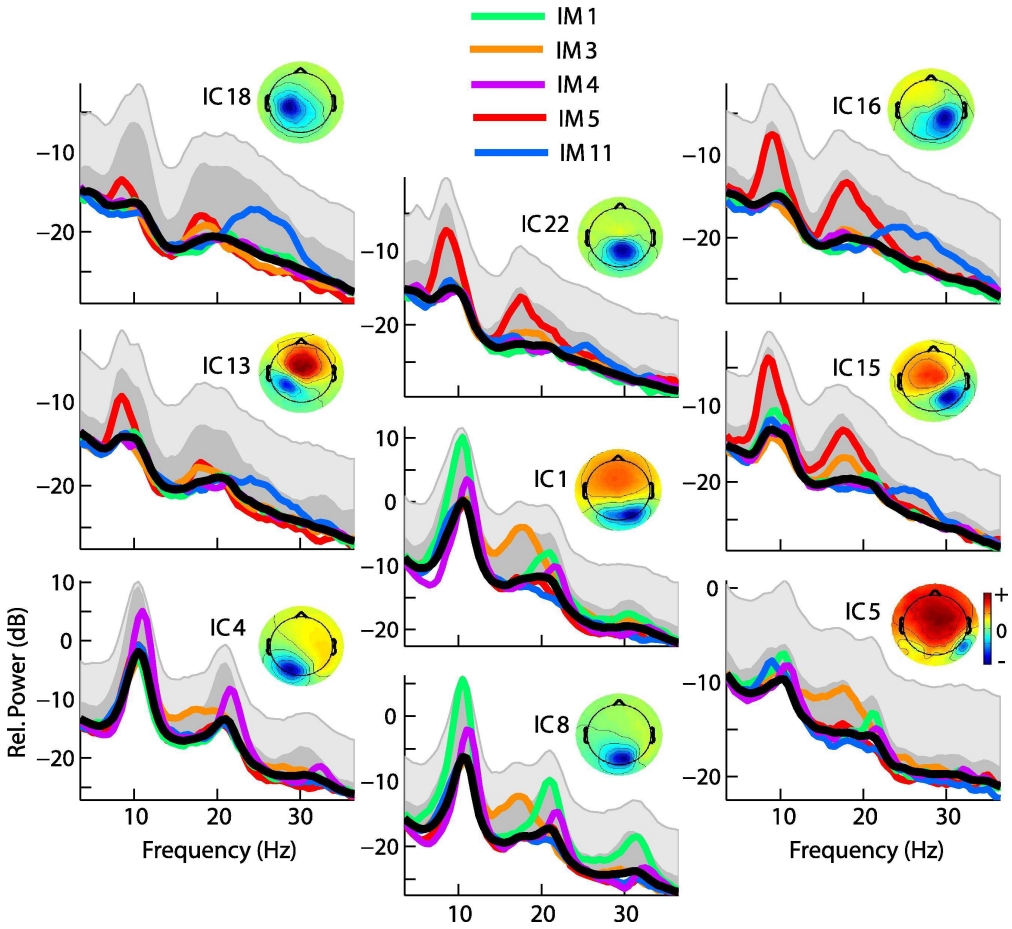

Figure 3. Maximal IM effects on IC power spectra. The maximal positive effects of five IMs (from Fig. 2) on the power spectra of nine ICs (colored traces), computed by back-projecting the highest positive time window weight for each IM and adding back the IC mean log-power spectrum (black traces). The upper borders of the grey areas show the (99th-percentile) maxima of raw power at each frequency, both in the entire IC data (lighter grey) and in the dimension-reduced data decomposed by ICA (darker grey). Note the various (here, positive) effects of the IMs on the IC spectra.

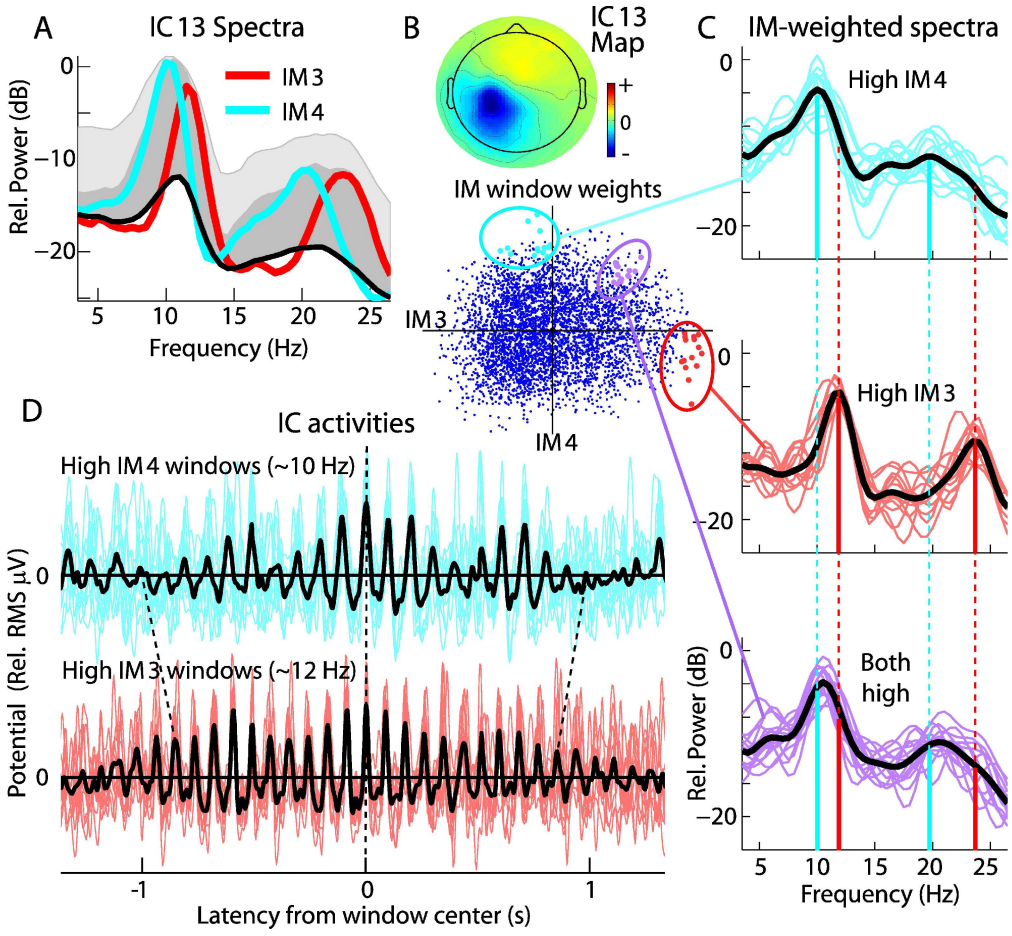

Figure 4. Multiple modulations of IC alpha band activity. A. Maximal spectral modulations (as in Fig. 3) for two alpha band modulators (IM3 and IM4) acting on a left somatomotor component (IC13) accounting for mu-rhythm activity across left parietal and frontal midline scalp (see map, B). B. Upper panel: Map of the IC13 scalp projection. Blue and yellow areas receive projections with opposite sign. Lower panel: Scatter plot of IM3 versus IM4 window weights. Red and light blue dots group time windows with dominant IM3 and IM4 weighting, respectively. Lavender dots show time windows positively weighted for both modulators. C. Colored traces show the IC13 power spectra for the selected time windows (from B). Black traces plot the means of the selected window spectra. Note the variations in peak alpha frequency between 10 Hz and 12 Hz, here modeled as reflecting the influences of IM3 and IM4. D. Light blue and red traces show 3 s of IC13 activity centered on the midpoints of the selected time windows (see B and C) and then aligned to their central upward-going central peaks. Black traces show the mean phase-aligned activations. The vertical dotted black line indicates the center of phase alignment and the slanted dotted lines, the Â±10 th local maxima in each mean waveform. The mean and single-trial activity waveforms are not sinusoidal, but rather are composed of sharp upward-going peaks and broad, blunted troughs, like the Greek letter mu (μ).

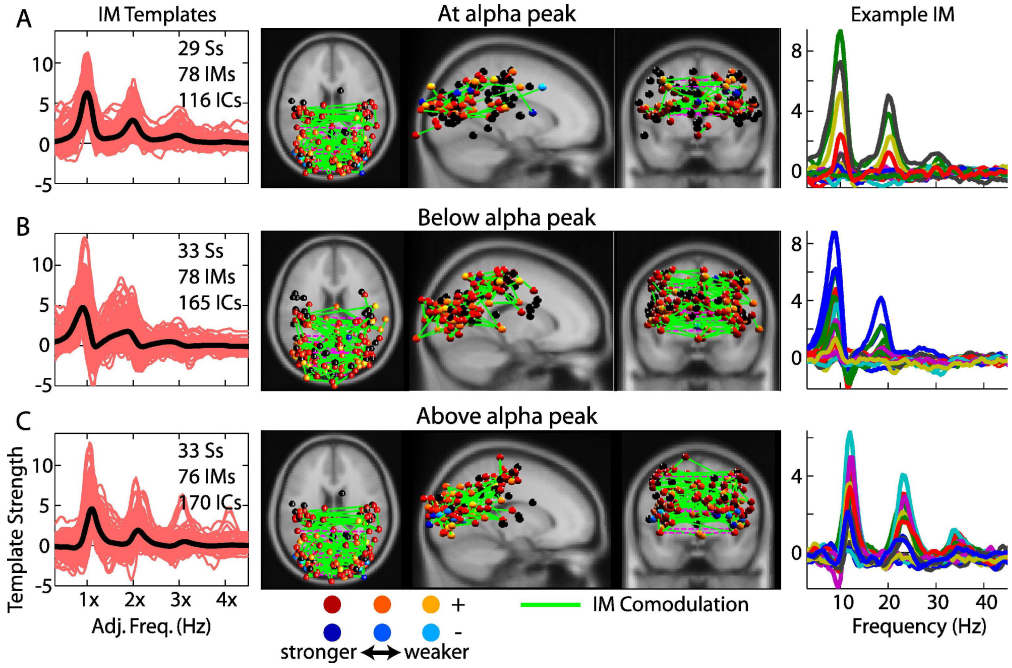

Figure 5. Alpha-band IM clusters. IMs for the 34 subjects were clustered based on similarities in power modulation templates. IM template frequency axes were linearly warped to align the respective IC mean alpha-band peak frequency to 1Ã□ (10 Hz). Red traces are clustered frequency-adjusted IM templates, and black traces their means. Mean MRI images show the 3-D distribution of equivalent dipole localizations of ICs contributing one or more IM templates to the cluster. Black balls are clustered IMs without co-modulates. Green lines connect co-modulated ICs (i.e., ICs with clustered templates belonging to the same IM). Warm-color balls indicate IC dipoles co-modulated with the same sign as the maximally modulated IC dipole; cool-color balls dipoles of ICs co-modulated with opposite sign. The three alpha-band IM clusters affected IC activity either at, below, or above the mean IC alpha peak frequency, respectively.

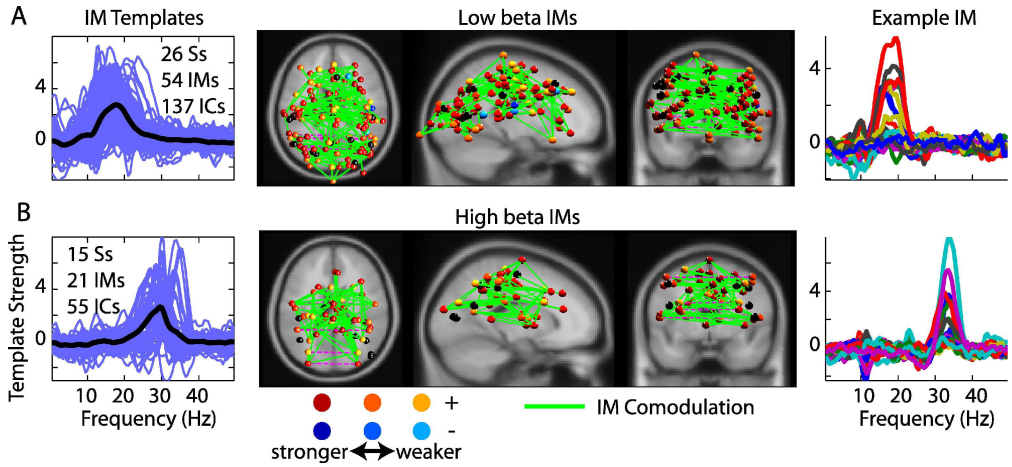

Figure 6. Beta-band IM clusters. Two clusters of beta-band modulators maximally affecting low beta (13-25 Hz) and high beta (25-35 Hz) activities respectively. (Left panels) Clustered IM templates (blue traces), and their means (black traces). (Center panels) 3-D distribution of equivalent dipole locations, as in Fig. 5, for ICs modulated by clustered IMs. (Right panels) Sample IM templates for each cluster.

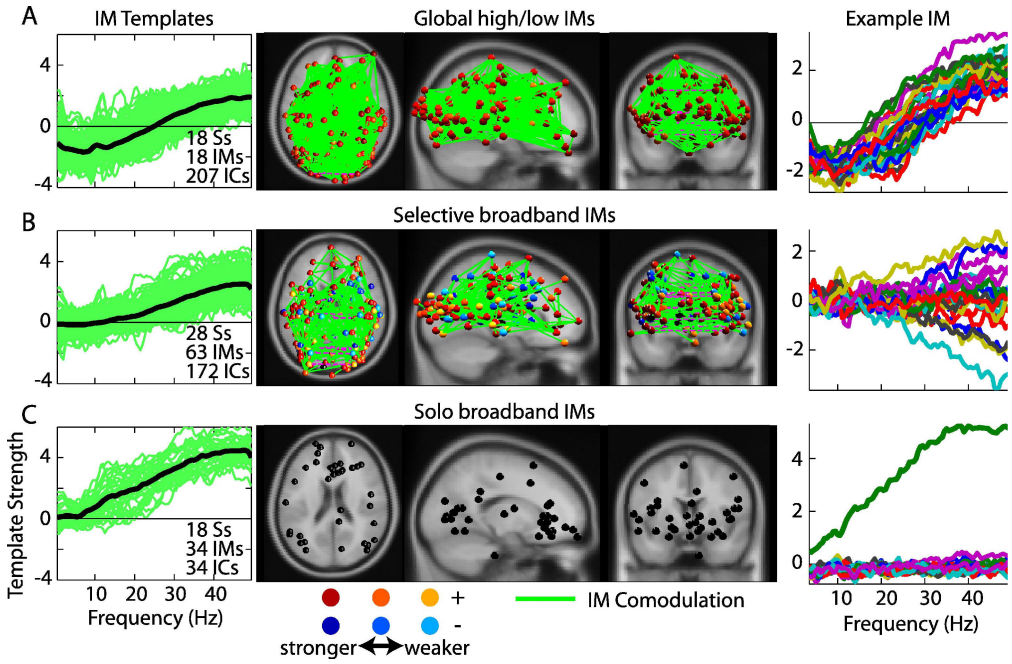

Figure 7. Broadband IM clusters. (Left panels) Broadband IM templates (green traces) and their means (black traces). (Center panels) Equivalent dipole distributions of modulated ICs (as in Fig. 5). (Right panels) Sample IM templates for each cluster. A. Global high/low cluster of IMs adjusting the ratio of high-frequency versus low-frequency power in all cortical ICs, with a mean frequency fulcrum near 25 Hz. B. Cluster of IMs that selectively co-modulated and/or spatially redistributed broadband power across several (but not all) IC, with stronger effects at higher frequencies. C. Cluster of IMs that increased or decreased broadband power above 5-10 Hz, and particularly above 30 Hz, in a single IC process.

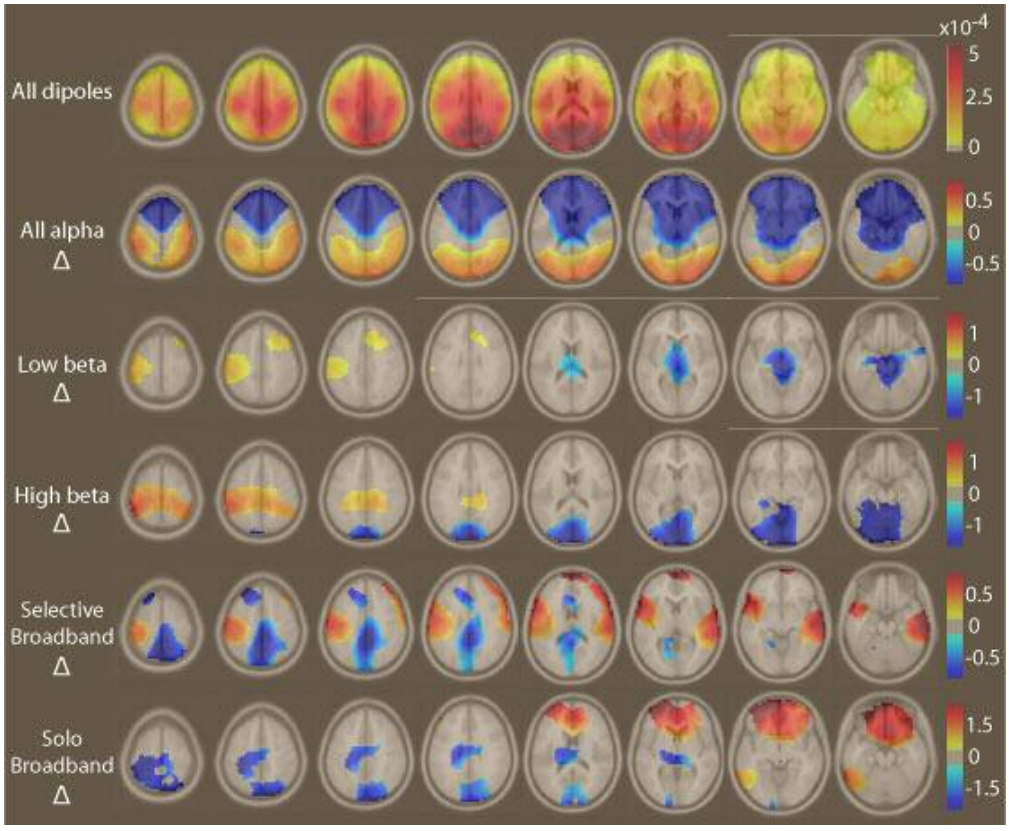

Figure S1. Spatial densities of independent modulator clusters. The top row shows the density of model dipoles for the dipolar independent component (IC) processes from 34 subjects used in the analysis. Color scale: Equivalent dipoles/subject/cc. Rows 2-7: Significant density differences from random selection for the noted IM clusters. Color scale: same as top row. Methods: To compute density, each dipole was replaced with a Gaussian cloud and then summed. Finally, results were scaled to dipoles/cc/subject. Rows 2-6 show significant dipole density differences from this distribution for ICs whose log spectra were modulated by IMs in the indicated IM clusters. Statistical significance of the observed density differences were estimated (at $p < .01$, not corrected for multiple comparisons) by drawing equal numbers of dipoles at random and computing the spatial density difference for this surrogate data. Repeating this process 500 times, sorting the resulting density difference values at each voxel, then noting the 1st and 99th percentiles values at each voxel, produced threshold images which were used to mask out non-significant density differences.

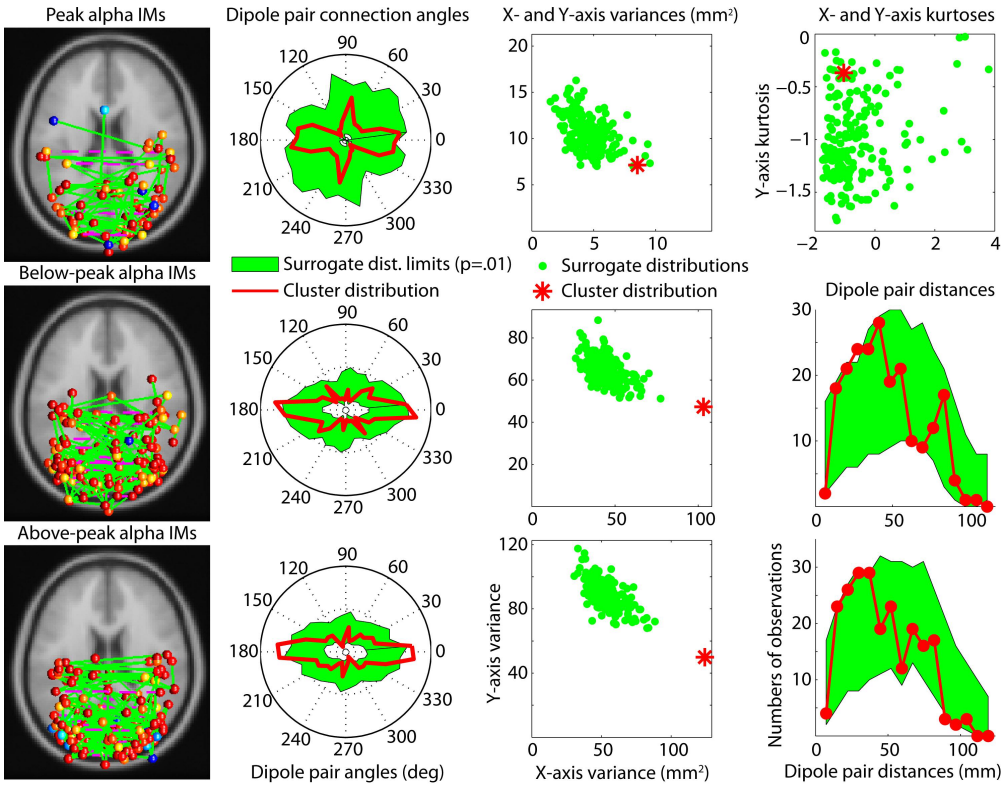

Figure S2. Model dipoles and connection statistics for the three alpha-band clusters. Left column: Equivalent dipole models (balls) and co-modulate connections (green lines). For details, see Fig. 5. second column. Polar angle histograms showing the distribution of axial plane angles of co-modulated equivalent dipole pairs (left column, red outlines). Green shapes show the 1st and 99th percentiles of surrogate data distributions created by randomly permuting the connections between cluster dipoles. Third column, red marks: Variance of the projection of the angle histograms (second column, red outlines) on the X (left-right) and Y (front-back) directions. Green spots: Variances of surrogate data histograms (see above). Note the large and highly significant dominance of the bilateral angle distributions for the off-peak alpha-band clusters (lower rows). Right column, red dots: Distributions of 3-D distances between co-modulated equivalent dipole pairs in the cluster. Green shapes: upper and lower limits represent 1st and 99th percentiles of the surrogate data distributions. Note the trend towards co-modulations involving nearby equivalent dipoles.

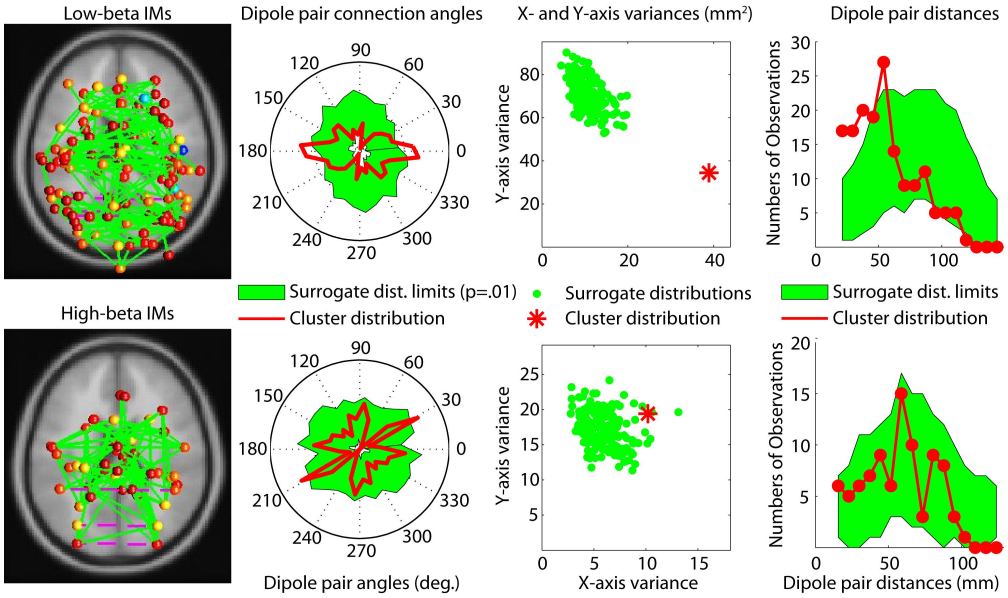

Figure S3. Model equivalent dipoles and co-modulated dipole pair statistics for the two beta-band clusters. As in Fig. S2. Note the dominance of bilateral dipole-pair connections for the low-beta band cluster (top middle columns) and the skew of the dipole-pair distance distribution towards short-range connections (upper right column).

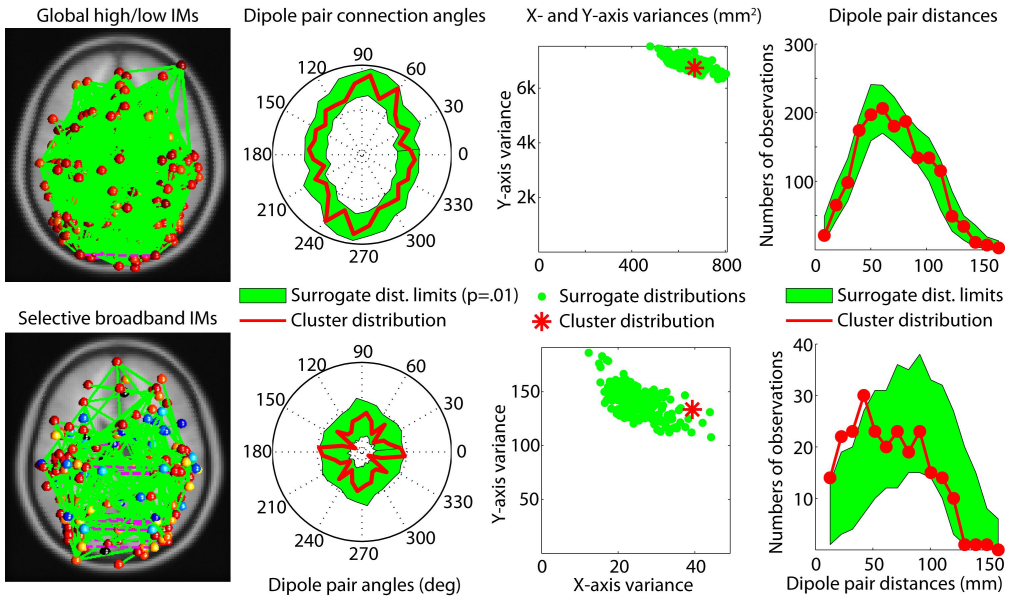

Figure S4 Model equivalent dipoles and co-modulated dipole-pair connection statistics for the two broadband clusters. As in Fig. S3. The global high/low cluster (upper row) contains all the dipoles for the 18 subjects represented in this cluster. For the selective broadband cluster (lower row), note the skew of the co-modulated equivalent dipole pair histogram (lower right panel) toward local connections, and the near dominance of bilateral connections (lower middle panels).

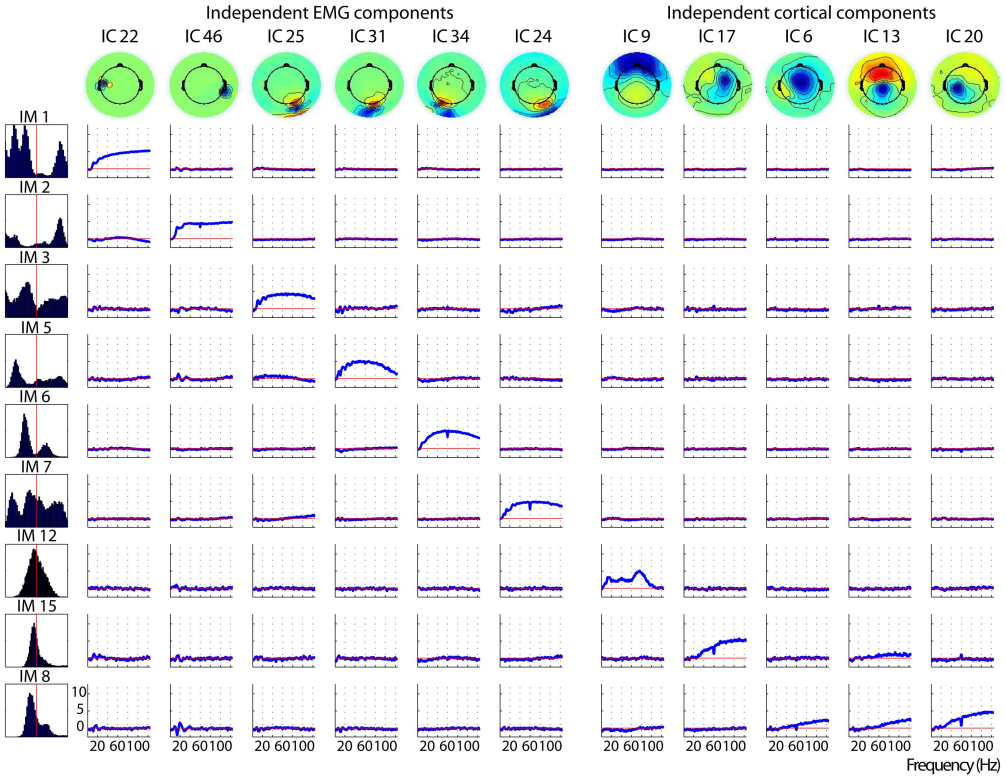

Figure S5. IM templates from a IM decomposition including cortical and electromyographic ICs with extended frequency range. Representative results of an IM decomposition for one subject including 23 ICs, 14 cortical components with near-dipolar scalp maps (some shown on right), plus 9 ICs accounting predominantly for scalp EMG activities, at frequencies between 1 Hz and 125 Hz. The illustrated broadband IMs either affect a single EMG IC (left) or one or more cortical ICs (right). Figure format as in main Fig. 2. Note the multi-peaked time-window weight histograms of the EMG components (left column) and the expected concentration of their spectral effects between 20 Hz and 100 Hz. Note, most importantly, the lack of effect of the EMG IMs on the cortical component spectra. Note, the sharp reductions at the line frequency, 60 Hz, from the broadband IM effects on cortical ICs. Checking the mean log spectra of these ICs confirmed the presence of similar-sized 60-Hz spikes in their power spectra in nearly all cases. The apparent deviance of the broadband IM templates at the line noise frequency (Fig. S5) likely reflects the lack of effect of these modulator processes on the remnant line noise in the cortical IC activations.

Guided Imagery Emotion Narratives

Positive Emotions (alternating, in random order, with negative emotions)

Awe □ You are standing at a vista point observing a scene of surpassing beauty, beginning to take it all in. Perhaps you are watching a sunset over the ocean, or tree-topped mountains stretching to the horizon. Or perhaps you are taking in the vastness of the Grand Canyon. As you view the glorious scene spread out before you, you are overcome by an amazing and all-encompassing feeling of complete and total awe at the beauty of creation. Allow this vision and feeling to permeate your entire being.

Compassion □ You are beginning to be filled with a feeling of loving concern for someone less fortunate than you who is suffering. Feel your body filling with intense sympathy and deep compassion for them. Perhaps you understand and sympathize with the suffering of a friend or loved one. Or perhaps you feel compassion for a stranger who is in trouble and is quietly calling out for love and understanding. Allow yourself to fully experience your compassion for their plight and suffering.

Contentment □ You are beginning to feel completely at ease. Your mood is calm and pleasant.. You feel everything is as it should be. Just now, you are facing no opposition. You feel everything is easy and graceful. You feel neither excited nor sad. You are filled with a pleasant and present feeling of contentment with everything. You enjoy this contented feeling as it pervades your entire body.

Excitement □ You are beginning to feel quick, energetic, uplifted. Perhaps you sense this is really your lucky day. Perhaps something you dreamed of experiencing is finally about to arrive, something that opens up new, exciting possibilities for you. You are finally getting your chance to experience something you have longed been looking forward to. Your body is filled with excitement that bubbles up and out of you in every direction.

Happiness □ You begin to feel a feeling of lightness and brightness enter you. You feel infused with cheerfulness. Your mouth wants to smile; your eyes take on an undeniable glimmer. Your feeling is one of full and complete happiness. Perhaps you imagine a perfect day□ the sun is shining and you are surrounded by your favorite friends, enjoying your favorite activity. Perhaps you are walking through a beautiful countryside, or are on your way to a special party. You have no worries. Your entire body is filled with idyllic happiness.

Joy □ You are beginning to sense a lightness in your being. You seem to want to smile. You have received outstanding news of something that fills your heart with pure joy. You could never have dreamt of being so fortunate. You feel practically like walking on air. Your feeling of blissful joy is pervasive and thrilling.

Love □ You begin to feel a bright glowing feeling of love welling up inside you. Perhaps your thoughts turn to someone you love dearly. Or perhaps you have a more general feeling of all-encompassing love for life, for truth, or for love itself. Invite this feeling of unconditional and enveloping love to fill a radiate from every part of your being.

Relief □ You are beginning to feel like taking a deep and relaxing plunge. You are free of the stress you were under. Perhaps you have just finished a long and difficult project. Or perhaps a pain or illness you were experiencing has just gone away. You feel a distinct and satisfying feeling of relief growing in you. Allow your body to become lightened and freed by this profoundly welcome feeling.

Negative Emotions (alternating, in random order, with positive emotions)

Anger □ Your heart is beginning to pound, your face feels warm and a feeling of distress is growing. You are feeling an intense and burning anger. Perhaps you remember an event in your life that caused uncontrollable anger to swell inside of you. Or perhaps you imagine an injustice□someone has demolished your car out of contempt, or your partner has betrayed you. Let this anger escalate inside of you.

Disgust □ You begin to feel revolted by what you are experiencing. Perhaps your face and stomach tighten as you open a can of food and find inside a festering mess that exudes a horrible smell. Perhaps you are exposed to a vile scene on TV or in real life. You feel an utter disgust that makes you want to run. But you cannot escape it; you must endure it while feeling of disgust fills your being.

Fear □ You are beginning to feel anxious and uneasy. You feel your breathing tighten and an emptiness in the pit of your stomach. You are gripped with real fear and cannot escape it. Perhaps you are physically threatened□your house is on fire, your boat is sinking, or an earthquake is shattering your home. Or, you are facing a frightening emotional challenge□a public speech, or an operation. For this short time, allow the imagined fear to dominate your being.

Frustration □ Something is not going as you would wish. You are beginning to feel agitated. Your body feels tense and uncomfortable, yet you feel helpless to change your situation. Perhaps your computer has crashed, deleting valuable files, or your ride to the airport is now an hour late. Or perhaps you are in a hurry but stuck in traffic. Gradually, you are overwhelmed with a profound and utter frustration. Let this feeling of frustration and annoyance affect your whole body.

Grief □ You are beginning to feel weighed down and leaden. Perhaps you have learned that a loved one has died unexpectedly. Perhaps your work has just collapsed, or your family dissolved. You feel a profound feeling of grief overwhelming you like a heavy weight. Your entire body is affected. Your heart is heavy, your mind anguished, your face sinks. Tears begin to gather. You can do nothing but endure this grief more and more until it eventually wears away.

Jealousy □ You are beginning to feel a seething, hateful feeling growing inside you. You feel troubled and uncomfortable as a fierce feeling of jealousy takes over. Perhaps your beloved is abandoning you for someone more beautiful or talented. Or, perhaps you are jealous of a peer whose work receives more praise than yours, or you see someone enjoying financial freedom you can only dream of Allow unrelenting jealousy to well up within you.

Sadness □ Your mood is beginning to become heavy. You feel lethargic and dull. Your forehead begins to droop and the corners of your mouth to turn downwards. Behind your eyes, tears begin to well up. You feel a profound and inescapable sadness. Perhaps you recall a sad scene from your life, or perhaps all your problems have become too much for you to handle and a deep sadness has captured you,. Allow the sadness to fill your body and mind.